MOBA based design of FOPID–SSSC for load frequency control of interconnected multi-area power systems

Ali Darvish Falehi[*]

Department of Electrical Engineering, Shadegan Branch, Islamic Azad University, Shadegan, Iran

Abstract. Automatic Generation Control (AGC) has functionally controlled the interchange power flow in order to suppress the dynamic oscillations of frequency and tie-line power deviations as a perturbation occurs in the interconnected multi-area power system. Furthermore, Flexible AC Transmission Systems (FACTS) can effectively assist AGC to more enhance the dynamic stability of power system. So, Static Synchronous Series Compensator (SSSC), one of the well-known FACTS devices, is here applied to accurately control and regulate the load frequency of multi-area multi-source interconnected power system. The research and efforts made in this regard have caused to introduce the Fractional Order Proportional Integral Derivative (FOPID) based SSSC, to alleviate both the most significant issues in multi-area interconnected power systems i.e., frequency and tie-line power deviations. Due to multi-objective nature of aforementioned problem, suppression of the frequency and tie-line power deviations is formularized in the form of a multi-object problem. Considering the high performance of Multi Objective Bees Algorithm (MOBA) in solution of the non-linear objectives, it has been utilized to appropriately unravel the optimization problem. To verify and validate the dynamic performance of self-defined FOPID–SSSC, it has been thoroughly evaluated in three different multi-area interconnected power systems. Meanwhile, the dynamic performance of FOPID–SSSC has been accurately compared with a conventional controller based SSSC while the power systems are affected by different Step Load Perturbations (SLPs). Eventually, the simulation results of all three power systems have transparently demonstrated the dynamic performance of FOPID–SSSC to significantly suppress the frequency and tie-line power deviations as compared to conventional controller based SSSC.

Keywords: power system dynamic stability; simultaneous optimization scheme; FOPID-SSSC; AGC; MOBA

1. Introduction

The size and complexity of the generation, transmission and distribution power systems have been continuously increased, and subsequently this problem has severely undermined the dynamic stability, power quality, protection systems of the interconnected multi-area power systems. For this reason, the frequency and inter-area tie-line power of interconnected multi-area power systems must be maintained within their nominal bounds via the required control design (Kazemi *et al.* 2007, Bevarani *et al.* 2008, Iracleus *et al.* 2005, Tan *et al.* 2009).

Therefore, each one not only controls its own production, but also controls its own load and schemed exchanges with adjacent areas. Since, the loads have been continual changed, thus, the frequency and tie-line power flows of the interconnected power system have been deviated from their nominal values. In this regard, a load frequency controller must be applied so that the frequency and inter-line power flows of the interconnected power system to be maintained in their stable values with the aim of enhance the power generation quality (Debbarma *et al.* 2014).

AGC has functionally operated to implicitly tune the output power of all units at various power plants with respect to the load variations. It can compensate the deviation in frequency and tie-line power exchange between areas as much as possible during the load perturbations and unscheduled operating conditions (Kundur *et al.* 1989). The main targets of AGC in the interconnected power systems can be expressed as follows:

(1) Suppress the dynamic oscillations of frequency and tie-line power deviations

(2) Good tracking performance without persistent oscillations throughout perturbation.

(3) Compensate the steady state value of frequency and tie-line power.

In accordance with the future power market, many different apparatuses with the considerable capacity and the rapid consumption of electricity would definitely create the great impacts. Due to lack of sufficient damping, the frequency oscillations can be situated within the inter-area modes of oscillation, following that continued and strengthened so that instability problem to be revealed (Falehi *et al.* 2012). For this reason, several scientific studies have been widely performed about the compensation capability of Flexible AC Transmission Systems (FACTS) to effectual control the power flow of transmission line. Due to the growing future power demand, FACTS devices not only increase the maximum power transfer in transmission line, but also augment the power

---

[*]Corresponding author, Ph.D.
 E-mail: a_darvishfalehi@sbu.ac.ir

system dynamic stability (Chaudhuri *et al.* 2003, Chaudhuri *et al.* 2004, Balarko *et al.* 2003, Gyugyi 1992, Falehi 2012, Falehi *et al.* 2011).

Static Synchronous Series Compensator (SSSC), the most effective and economical member among the FACTS series compensators, has considerably augmented the power system dynamic stability (Cai *et al.* 2005). As a result of an adjustable Voltage Source Converter (VSC), SSSC can virtually compensate the impedance of transmission line (Falehi *et al.* 2011, Panda *et al.* 2010). Over the past two decades, many kinds of controllers have been introduced for SSSC in order to suppress the dynamic oscillations of frequency and tie-line power deviations in the disturbed interconnected power systems (Truong *et al.* 2015, Panda 2011, Bhatt *et al.* 2011). What is certain is that any fault occurrence or severe operating condition and the like in power lead to the instability of power system. Thus, presence of a high performance controller for SSSC has significantly enhanced its compensation capability to suppress the power system dynamic oscillations, and also retrieve the power system into the stable status.

In recent years, several controllers apart from conventional controllers e.g. Fuzzy Logic Controller (FLC), Neuro Fuzzy Inference System (ANFIS), Sliding Mode Controller (SMC) and the same have equipped the SSSC to enhance the power system stability (Khuntia *et al.* 2013, Truong *et al.* 2015, Swain *et al.* 2015, Taibin *et al.* 2011). Despite that, the conventional controllers e.g., Proportional Integral Derivative (PID) for their simplicity and abstain from the complexity, they are still being preferred and applied in the power system and relevant industries. Not that, the behavior of controllers and systems has been modeled using integer order, provided they can be more appropriately and actually constructed with respect to fractional calculus. But then, the "Commande Robuste Order Non Entier (CRONE)" control strategy is introduced as non-integer or fractional order robust control (Sabatier *et al.* 2015). Inspired by this idea, the efficiency of the PID controller has been improved using assistance of fractional calculus. Fractional calculus has positively provided an appropriate tool to construct the Fractional Order (FO) of integrals and derivatives (Xue *et al.* 2002, Zamani *et al.* 2009, Alomoush 2010, Lu *et al.* 2012). When all is done, Fractional Order Proportional Integral Derivative (FOPID) is introduced for SSSC as dynamic oscillation damper. The self-defined FOPID–SSSC is functionally operated in order to augment the dynamic stability of power system.

Since both the frequency and tie-line power deviations must be simultaneously suppressed, minimization of both these functions is formularized in the form of a multi-object problem. Considering the MOBA in solution of the non-linear objectives, it has been utilized to appropriately unravel the optimization problem.

The dynamic performance of FOPID–SSSC has been thoroughly evaluated in three different multi-area interconnected power systems, that is to say three-area hydro-thermal, two-area hydro-thermal-diesel and IEEE 39-bus New England power systems. To verify and validate the FOPID–SSSC performance, all three aforementioned power systems have been affected by Step Load Perturbation (SLP). Furthermore, MOBA based simultaneous optimization scheme has been performed with respect to occurrence of SLP in all areas of the interconnected power systems. Meanwhile, the dynamic performance of FOPID–SSSC has been accurately compared with a conventional controller based SSSC. To sum up, the simulation results of all three power systems have corroborated the dynamic performance of FOPID–SSSC in order to suppression of the frequency and tie-line power deviations as compared to conventional controller based SSSC.

2. Multi-objective bees algorithm

2.1 BA Review

BA, as one of the swarm intelligence based heuristic algorithms, has been constructed with respect to the natural foraging behavior of honey bees to identify and acquire the nectar and pollen from flowering herbs, shrubs and trees. This algorithm had been firstly developed by Prof. Duc Truong Pham and his colleagues at Cardiff University (Pham *et al.* 2006), following that, it has been implemented to solve the single objective problems (Pham *et al.* 2006). An upgraded version of BA has been constructed so that many non-dominated solutions to be identified (Pham *et al.* 2006). Note that, the multi objective problem is more unfathomable as compared to the single objective problem. By means of its multi-objective type, an efficacious solution set recognized as Pareto optimal solutions would be created to provide an optional determinative with more flexibility, and then extraction of an appropriate alternative.

2.2 Natural foraging procedure of bees

Bee colony occupies a portion of its flock in vintage duration to make a reconnaissance of the patches surrounding the beehive (Tereshko *et al.* 2005). Scout bees have stochastically foraged to obtain the nectar sources. During the time back to the beehive, they accumulate the nectar as have been achieved in the foraging process time. Afterwards, scout bees are beginning to carry out the ceremonial practice called "waggle dance" to make relationship with other bees and transmit the relevant information about nectar sources to them (Pham *et al.* 2006). The waggle dance has been executed in a specific patch surrounding the beehive that called "dance floor" which transmits three substantial parts of information with respect to the flowering plants: its direction (in accordance with the angle between sun and its location), its distance from the beehive (continuity of dance), and its quality (frequency of dance) (Pham *et al.* 2009). Following that, dancer bee returns to the flowering plants and inform the recruited bees. Their number is highly depends on the quality of plants. In fact, the flowering plants that encompass affluent and readily available nectar sources will allure and catch lots of foragers. Once again, one of the recruited foragers comes back to the beehive, and successively carries out the waggle dance provided that other idle bees to be motivated towards the nectar source

(Tereshko *et al.* 2005, Pham *et al.* 2009).

2.3 Bees algorithm construction

Some parameters of BA which should be initially set are: number of scout bees, number of sites chosen for neighborhood search, number of top-rated sites i.e. elite among m chosen sites, number of bees recruited for the best elite sites, number of bees recruited for other chosen sites, initial size of each patch, and stopping criterion (Moradi *et al.* 2014). Also, BA flowchart in the form of multi-objective configuration is presented in Fig. 1:

2.4 Fundamental conceptions of multi objective optimization problem

General multi-objective functions can be introduced by: Minimize X

$$f(X)=[f_1(X),f_2(X),...,f_k(X)] \tag{1}$$

Subject to

$$g_i(x) \leq 0 \ ; \ i = 1, 2,...,m \tag{2}$$

$$h_j(x) = 0 \ ; \ j = 1, 2,...,p \tag{3}$$

Where $X=[X_1,X_2,...,X_n]^T$ Which is variables' vector, f_i, $i = 1, 2,...,k$ indicates the objective functions and g_i, h_j, $i = 1, 2,...,m$, $j = 1, 2,...,p$ indicates the problem's limitations
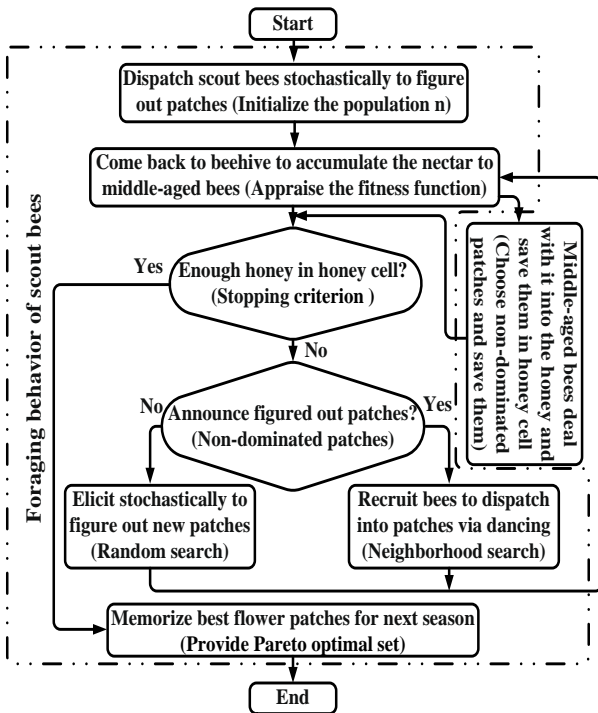

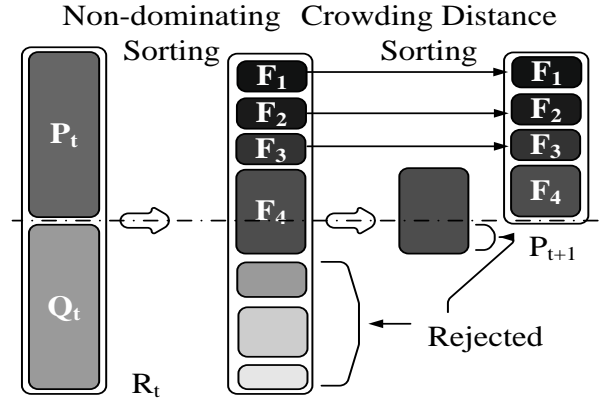Fig. 1 Flowchart of non-dominated sorting MOBA

Fig. 2 Mechanism of selection based on non-dominated sorting MOBA

The optimization problems based on multi-objective have been actually constructed in order to figure out an appropriate trade-off. The concept of Pareto Front/Surface can be presented by some following determinations:

Determination 1. Crate two vectors $X,Y \in \mathfrak{R}^n$, is referred to $X \leq Y$ if $x_i \leq y_i$ for $i = 1, 2,...,k$, and that X dominates Y (pointed to by $X \prec Y$) if $X \leq Y$ and $X \neq Y$.

Determination 2. Expressed that a vector resolution variables $X \in \chi \subset \mathfrak{R}^n$ is non-dominated according to χ , provided no $X' \in \chi$ to the extent that $f(X') \prec f(X)$.

Determination 3. Expressed that a vector of resolution variables $X^* \in F \subset \mathfrak{R}^n$ (F indicate expedient area) is Pareto optimal provided to be non-dominated according to F .

Determination 4. The Pareto Optimal Set P^* is defined as follows

$$P^* = \{X \in F \,/\, X \text{ is Pareto optimal}\} \tag{4}$$

Determination 5. The Pareto Front PF^* is defined as follows

$$PF^* = \left\{f(X) \in \mathfrak{R}^k \mid X \in P^*\right\} \tag{5}$$

2.5 Non-dominated sorting bees algorithm principle

Non-dominated Sorting Bees Algorithm (NSBA) has scholastically created the spread out initial population *P* of N_P solutions. A recruited bee provides an adaptive position in its mind contingent upon the ocular information and tastes and evaluates the nectar size and quality of the new source. Following the adaptation procedure, the parent and offspring will be merged to construct the population R_t

$$R_t = P_t \cup Q_t \quad \text{that} \quad size\left(R_t\right) = 2N_P \tag{6}$$

Then, the future population utilized by spectator bees P_{t+1} is created by selecting the best N_P solutions of the combined population R_t. Every solution is dealt with via its class status as a primary principle and also crowding

distance as secondary. The class status is performed according to the non-domination (Chakraborty *et al.* 2009). A spectator bee deals with the nectar information thorough the recruited bees and engages a nectar sources according to the related probability with nectar source that can be presented as follow

$$p_i = {D_i}/{N_P} \qquad (7)$$

Where, D_i is the solution number dominated by i solution. Here, spectator bee creates an adaptation on the position i.e., solution in its mind and controls the nectar value of the nominated source i.e., solution. Neighborhood nectar source X'_i can be presented by

$$X_i^{'} = \left(x_{i0}, x_{i1}, x_{i2}, \dots, x_{i(j-1)}, x'_{ij}, x_{i(j+1)}, \dots, x_{i(D-1)}\right) \qquad (8)$$

The value of x'_{ij} in $X_i^{'}$ solution can be calculated by:
$$x'_{ij} = x_{ij} + u\left(x_{ij} - x_{kj}\right) \quad j \in [0, D-1] \ , \ k \in [0, N_P - 1] \ , \ k \neq i \ , \ u \in [-1, 1]$$

The whole parent and offspring subsequent to the obtaining modified by spectator bees are merged to configure the combined population. Eventually, the individuals extracted by the combined population can be presented in Fig. 2.

3. Theory and design of FOPID–SSSC

3.1 Fractional order theory

The Fractional Order (FO) control principle surveys the differential equations taken from fractional calculus model. It deals with the concept of $d^n y(t) dt^{-n}$ and $d^\alpha y(t) dt^{-\alpha}$ with n and α which are integer and non-integer (even complex possibility) numbers, respectfully. Non-integer order factor $_a D_t^\alpha$ provides the Fractional Order (FO) factor of derivative and integral, hither, a (conventionally is zero) and t are the constrains that it can be expressed as follows (Sabatier *et al.* 2015)

$$_a D_t^\alpha = \begin{cases} {d^\alpha}/{dt^\alpha} & \Re(\alpha) > 0 \\ 1 & \Re(\alpha) = 0 \\ \int_a^t (d\tau)^\alpha & \Re(\alpha) < 0 \end{cases} \qquad (9)$$

Accordingly, based on Riemann–Liouville definition, for derivative

$$_a D_t^\alpha f(t) = \frac{1}{\Gamma(n-\alpha)} {d^n}/{dt^n} \int_a^t \frac{f(\tau)}{(t-\tau)^{1-(n-\alpha)}} d\tau \qquad (10)$$

Also, for integral

$$_a D_t^{-\alpha} f(t) = \frac{1}{\Gamma(\alpha)} \int_a^t \frac{f(\tau)}{(t-\tau)^{1-\alpha}} d\tau \qquad (11)$$

For $n-1 \leq \alpha < n$ and $\Gamma(.)$ is the Euler's gamma function. Laplace transformation of fractional derivative is

$$L\left\{_a D_t^\alpha f(t)\right\} = s^\alpha F(s) - \sum_{k=0}^{n-1} s^k D_t^{\alpha-k-1} f(t)|_{t=0} \qquad (12)$$

The FO of s-domain can be approximated using a non-integer order transfer function in the pre-defined frequency range $[\omega_l, \omega_h]$. Among the relevant approximations, Crone approximation is usually opted owing to the common trends (Sabatier *et al.* 2015). This approximation provides zeros and poles, i.e.

$$s^\alpha \approx K \prod_{n=1}^N \frac{1 + \left({s}/{\omega_{z,n}}\right)}{1 + \left({s}/{\omega_{p,n}}\right)} \qquad (13)$$

Where, K is an adapted gain, and N is number of poles and zeros. Whenever N increases, the approximation will be intricate. Also, pre-defined parameters of equation can be represented

$$\varepsilon = \left({\omega_h}/{\omega_l}\right)^{{\alpha}/{n}} , \quad \eta = \left({\omega_h}/{\omega_l}\right)^{{(1-\alpha)}/{n}} \qquad (14)$$

The recursively attained parameters

$$\omega_{z,1} = \omega_n \sqrt{n} \ , \quad \omega_{p,n} = \omega_{z,n} \varepsilon \ , \quad \omega_{z,n+1} = \omega_{p,n} \sqrt{\eta} \qquad (15)$$

It is worth mentioning that, FO of linear dynamic system can be represented by a FO linear differential equation (Lu 2012)

$$\begin{aligned} &a_n D_t^{\alpha_n} y(t) + a_{n-1} D_t^{\alpha_{n-1}} y(t) + \dots + a_0 D_t^{\alpha_0} y(t) = \\ &b_m D_t^{\beta_m} u(t) + b_{m-1} D_t^{\beta_{m-1}} u(t) + \dots + b_0 D_t^{\beta_0} u(t) \end{aligned} \qquad (16)$$

Using Laplace transformation considering a=0, the transfer function of the FO system can be expressed as follows

$$G(s) = \frac{b_m s^{\beta_m} + b_{m-1} s^{\beta_{m-1}} + \dots + b_0 s^{\beta_0}}{a_n s^{\alpha_m} + a_{n-1} s^{\alpha_{m-1}} + \dots + a_0 s^{\alpha_0}} \qquad (17)$$

3.2 FOPID controller

Here, $PI^\lambda D^\mu$ represents FOPID controller with following transfer function

$$G_c(s) = K_p + K_i s^{-\lambda} + K_d s^\mu \qquad (18)$$

Where, λ and μ are the FO of integrator and derivative, respectively. Despite problem complexity, these parameters can enhance the flexibility of this controller. To better conceive these statements, Fig. 3 is presented to demonstrate different categories of integer and non-integer order controllers so that λ and μ change. As previously mentioned, SSSC is hither implemented to assist AGC in

order to suppress the dynamic oscillations of frequency and tie-line power deviations in the disturbed interconnected power systems.

In this regard, it is impressive that a high performance controller to be introduced for SSSC. As a result, FOPID controller is designed and implemented for SSSC to appropriately control the power flow. But then, the following advantages of FO controllers as compared to integer order controllers can be expressed as follows:

• Robustness against parameters variation.
• High efficiency for existence of two additional variables, and accordingly enhance overall system freedom degree.

Considering these advantages, FOPID–SSSC based on MOBA has been optimally effectuated.

4. Interconnected multi source multi area power systems integrated with FOPID–SSSC

4.1 SSSC Linearization related to AGC

SSSC is generally occupied a self-adaptive VSC to generate the required three phase voltage orthogonal with the current of transmission line, withal operating in capacitive or inductive mode reactance in order to control the power flow in transmission lines. By means of regulating the feed voltage's magnitude (V_q) considering its polarity, the compensation level is dynamically adjusted, and then the capacitive or inductive mode would be obtained (Gyugyi *et al.* 1997).
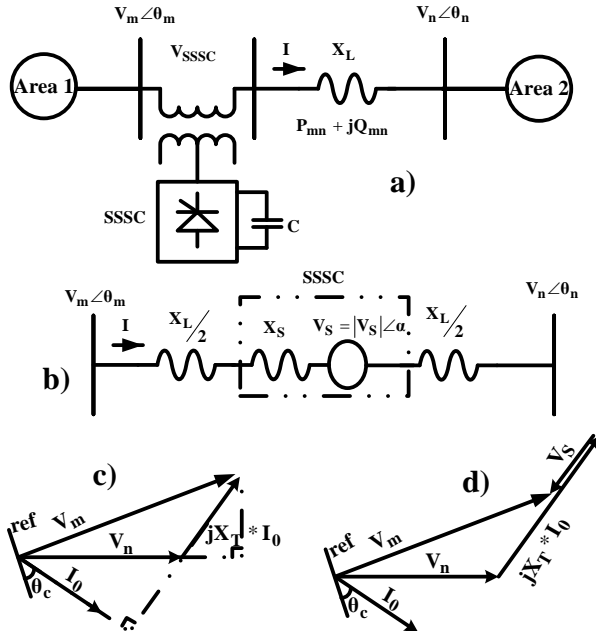

Fig. 4 (a) schematic of the selected two-area from interconnected power system with consideration of SSSC, (b) the power system equivalent circuit with consideration of SSSC, (c) phasor diagram and (d) 90° difference between current angle and voltage angle

Two areas of an interconnected multi area power system are hither engaged to carry out the linearization procedure with consideration of SSSC in series with the tie-line, whereby, its single-line diagram is given in Fig. 4(a). Since the tie-line resistance value is much fewer than its inductance value, hence, the resistance value can be overlooked. Based on quickly control of power flow suing SSSC, this device is here applied to alleviate dynamic oscillations of frequency and tie-line power deviations. As for the equivalent circuit of test power system presented in Fig. 4(b), SSSC is conventionally introduced by the series voltage source (Vs) accompanied by the leakage reactance of transformer Xs. Meanwhile, the relevant phasor diagram of the power system taking into account the SSSC operational conditions is shown in Figs. 4 (c) and (d). Note that, the voltage of SSSC (V_S) just controls the current amplitude with no altering of its angle. Considering phasor diagram given in Fig. 4(c), system current flow (I_0) can be attained as follows

$$I_0 = \frac{V_m \angle \theta_m - V_n \angle \theta_n}{jX_T} \qquad (19)$$

Where, $X_T = X_L + X_S$. The current angle can be also attained by

$$\theta_c = \sin^{-1}\left(\frac{V_n \cos \theta_n - V_m \cos \theta_m}{\sqrt{V_n^2 + V_m^2 - 2V_nV_m \cos \theta_{mn}}}\right) \qquad (20)$$

Where, $\cos \theta_{mn} = \cos(\theta_m - \theta_n)$
Considering SSSC, Eq. (19) is turned into

$$I = \frac{V_m \angle \theta_m - V_S \angle \alpha - V_n \angle \theta_n}{jX_T} =$$
$$\left[\frac{V_m \angle \theta_m - V_n \angle \theta_n}{jX_T}\right] + \left[-\frac{V_S \angle \alpha}{jX_T}\right] = I_0 + \Delta I \qquad (21)$$

ΔI indicates a complemental current part being the SSSC i.e., Vs .

The tie-line power between m and n can be formulized as follows

$$S_{mn} = V_m I^* = S_{mn0} + \Delta S_{mn}$$
$$P_{mn} + jQ_{mn} = (P_{mn0} + \Delta P_{mn}) + j(Q_{mn0} + \Delta Q_{mn}) \qquad (22)$$

Active and reactive power are respectively indicated by P_{mn0} and Q_{mn0} without considering SSSC i.e., V_S is zero. With no consideration of the SSSC, it can be relatively formulized by

$$\Delta P_{mn} = \frac{V_m V_S}{X_T} \sin(\theta_m - \alpha) \qquad (23)$$

As V_S is perpendicular to I ($\alpha = \theta_c - \pi/2$), ΔP_{mn} can be represented by

$$\Delta P_{mn} = \frac{V_m V_S}{X_T} \cos(\theta_m - \theta_c) \qquad (24)$$

Since, SSSC has no any active power exchange with system, ΔP_{mn} in both sides of SSSC would be alike, that is to say

$$\Delta P_{mn} = \frac{V_m V_S}{X_T}\cos(\theta_m - \theta_c) = \frac{V_n V_S}{X_T}\cos(\theta_n - \theta_c) \quad (25)$$

Abovementioned equal relationship is simplified as follows

$$\cos(\theta_m - \theta_c) = \frac{V_n}{V_m}\cos(\theta_n - \theta_c) \quad (26)$$

Considering Fig. 4(c), $\cos(\theta_n - \theta_c)$ can be calculated

$$\cos(\theta_n - \theta_c) = \frac{V_m\sin\theta_{mn}}{\sqrt{V_n{}^2 + V_m{}^2 - 2V_nV_m\cos\theta_{mn}}} \quad (27)$$

ΔP_{mn} with respect to aforementioned equation is turned into

$$\Delta P_{mn} = \frac{V_n V_S}{X_T} * \frac{V_m\sin\theta_{mn}}{\sqrt{V_n{}^2 + V_m{}^2 - 2V_nV_m\cos\theta_{mn}}} \quad (28)$$

From (22)

$$P_{mn} = P_{mn0} + \Delta P_{mn} = \frac{V_nV_m}{X_T}\sin\theta_{mn} +$$

$$\frac{V_nV_m}{X_T}\sin\theta_{mn}\frac{V_S}{\sqrt{V_n{}^2 + V_m{}^2 - 2V_nV_m\cos\theta_{mn}}} \quad (29)$$

By means of linearization around the operating point

$$\Delta\dot{P}_{mn} = \frac{V_nV_m}{X_T}\cos(\theta_m - \theta_n)(\Delta\theta_m - \Delta\theta_n) +$$

$$\frac{V_nV_m}{X_T}\sin\theta_{mn}\frac{\Delta V_S}{\sqrt{V_n{}^2 + V_m{}^2 - 2V_nV_m\cos\theta_{mn}}} \quad (30)$$

$$\Delta\dot{P}_{mn} = T_{mn}(\Delta\theta_m - \Delta\theta_n) + K_v\Delta V_S \quad (31)$$

Where, $\quad T_{mn} = \dfrac{V_mV_n}{X_T}\cos(\theta_m - \theta_n)$, and

$$K_v = \frac{V_nV_m}{X_T}\sin\theta_{mn}\frac{1}{\sqrt{V_n{}^2 + V_m{}^2 - 2V_nV_m\cos\theta_{mn}}}$$

Since:

$$\Delta\theta_m = \int\Delta\omega_m.dt, \quad \Delta\theta_n = \int\Delta\omega_n.dt$$

$$\Delta\dot{P}_{mn} = T_{mn}\left[\int\Delta\omega_m.dt - \int\Delta\omega_n.dt\right] + K_v\Delta V_S \quad (32)$$

The Laplace transformer of Eq. (32) will be

$$\Delta\dot{P}_{mn}(s) = T_{mn}\Big/s\,[\Delta\omega_m(s) - \Delta\omega_n(s)] + K_v\Delta V_S(s) \quad (33)$$

Considering Eq. 31, ΔV_S term functionally controls

and regulates the active power of tie-line. Pertinent controller that modifies the voltage of SSSC is eventually presented by

$$\Delta V_S = \left(\frac{1+T_1S}{1+T_2S}\right)\left(\frac{1+T_3S}{1+T_4S}\right)\left(\frac{K_s}{1+T_{SSSC}S}\right)\Delta\omega(s) \quad (34)$$

In accordance with the abovementioned relationship, $\Delta\omega(s)$ should be received and applied as SSSC's supplementary signal in order to modify V_S, and then control the active power among these areas withal alleviate the dynamic oscillations of frequency and tie-line power deviations. Ergo

$$\Delta\dot{P}_{mn}(s) = T_{mn}\Big/s\,[\Delta\omega_m(s) - \Delta\omega_n(s)] +$$

$$K_v\left(\frac{1+T_1S}{1+T_2S}\right)\left(\frac{1+T_3S}{1+T_4S}\right)\left(\frac{K_s}{1+T_{SSSC}S}\right)\Delta\omega_i(s) \quad (35)$$

$$\Delta\dot{P}_{mn}(s) = \Delta P_{mn}^0(s) + \Delta P_{SSSC}(s) \quad (36)$$

Where,

$$\Delta P_{SSSC}(s) = K_{SSSC}\left(\frac{1+T_1S}{1+T_2S}\right)\left(\frac{1+T_3S}{1+T_4S}\right)\left(\frac{1}{1+T_{SSSC}S}\right)\Delta\omega_i(s)$$

, and $\quad K_{SSSC} = K_v * K_s$

From the viewpoint of dynamic stability, $\Delta\omega$ should be chosen and fed into the conventional controller. Based on Eq. (35), this controller is structured using double lead-lag structures for compensating the phase considering time constants of: T_1, T_2, T_3 and T_4, withal a lag structure considering time constant of T_{SSSC} along with gain of K_{SSSC}. As described in previous section, FOPID–SSSC is suggested to the augment the power system dynamic stability. In this regard, second term of the tie-line power exchange relationship with presence of the fractional order based controller can be represented by

$$\Delta P_{SSSC}(s) = \left(K_{P,SSSC} + K_{I,SSSC}S^{-\lambda} + K_{D,SSSC}S^{\mu}\right)\Delta\omega_i(s) \quad (37)$$

4.2 Three-area hydro-thermal linearization

As previously explained, AGC can properly perform its function soon as occurrence of a slow and small load changes. Hence, the nonlinear power system must be linearized as for the slight load variations at operating point. When all is done, the single-line diagram of this power system integrated with SSSC is given in Fig. 5(a). Since, the tie-line resistance value is too small with respect to the tie-line inductance, it is here overlooked. This system is generally constructed by three identical areas of generation, i.e., double reheat thermal are dedicated for first and second area, withal hydro for third area. The steam turbine's configuration and hydro turbine's configuration are unalike from the several respects. Generation Rate Constraint (GRC) is taken to be 3% per minute for thermal area, 4.5% per second for upper and 6% per second for lower hydro

area. All areas of the power system have 2000 MW identical generation capacity. Likewise, both the thermal and hydro areas encompass bias setting (B_i). a_{12}, a_{13} and a_{23} rating factors of the power system provided the relevant relationships considering tie-line power deviation are drown out using the following trend:

Thermal areas

$$\Delta f_i(s) = \frac{K_{pi}}{1+sT_{pi}}\left[\Delta P_{Gi}(s) - \Delta P_{Di}(s) - \Delta P_i(s)\right] \quad (38)$$

$$\Delta P_{Gi}(s) = \frac{1+sK_{ri}T_{ri}}{T_{ri}}\Delta P_{Ri}(s) \quad (39)$$

$$\Delta P_{Ri}(s) = \frac{1}{1+sT_{ti}}\Delta x_{Ei}(s) \quad (40)$$

$$\Delta P_{refi}(s) = -G_{AGC,i}(s)\left[B_i(s)\Delta f_i(s) + \Delta P_i(s)\right] \quad (41)$$

$$\Delta x_{Ei}(s) = \frac{1}{1+sT_{gi}}\left[\Delta P_{refi}(s) - \frac{1}{R_i}\Delta f_i(s)\right] \quad (42)$$

While, *i* represents the number of thermal area *(i=1, 2)*.

Hydro area

$$\Delta f_3(s) = \frac{K_{p3}}{1+sT_{p3}}\left[\Delta P_{G3}(s) - \Delta P_{D3}(s) - \Delta P_3(s)\right] \quad (43)$$

$$\Delta x_{E3}(s) = \frac{K_d.s^2 + K_p.s + K_i}{K_d.s^2 + \left(K_p + \frac{1}{R_3}\right).s + K_i} \\ \left[\Delta P_{ref3}(s) - \frac{1}{R_3}\Delta f_3(s)\right] \quad (44)$$

$$\Delta P_{G3}(s) = \frac{1-sT_W}{1+0.5sT_W}\Delta P_{R3}(s) \quad (45)$$

$$\Delta P_{ref3}(s) = -G_{AGC,3}(s)\left[B_3(s)\Delta f_3(s) + \Delta P_3(s)\right] \quad (46)$$

Tie-line power deviations can be also determined by

$$\Delta P_{12}(s) = \frac{2\pi T_{12}}{s}\left(\Delta f_1(s) - \Delta f_2(s)\right) \quad (47)$$

$$\Delta P_{23}(s) = \frac{2\pi T_{23}}{s}\left(\Delta f_2(s) - \Delta f_3(s)\right) \quad (48)$$

$$\Delta P_{31}(s) = \frac{2\pi T_{31}}{s}\left(\Delta f_3(s) - \Delta f_1(s)\right) \quad (49)$$

And also

$$\Delta P_1(s) = \Delta P_{12}(s) + \alpha_{31}\Delta P_{31}(s) \quad (50)$$

$$\Delta P_2(s) = \alpha_{12}\Delta P_{12}(s) + \Delta P_{23}(s) \quad (51)$$

$$\Delta P_3(s) = \alpha_{23}\Delta P_{23}(s) + \Delta P_{31}(s) \quad (52)$$

Further information about this power system is detailed in Appendix A.

4.3 Two-area hydro-thermal-diesel linearization

The linearized interconnected power system is presented in Fig. 5(b). In this power system, GRC is taken 10% per minute for thermal area and 4.5% per second for upper and 6% per second for lower hydro area. This system encompasses two dissimilar areas i.e., capacities of 1800 MW and 1200 MW are considered first and second areas that both of them have hydraulic unit. Further information about this power system is detailed in Appendix B.

4.4 IEEE 39-bus 10-machine New England System

IEEE 39-bus power system which is well-known as 10-machine New England Power System is considered to more evaluate the dynamic performance FOPID–SSSC. It has been generally constructed by thirty nine busses, ten generators, nineteen loads, and twenty nine transmission lines and twelve transformers. This multi-machine power system has been widely applied as a test system to verify the performance of new controllers and strategies over the years. Fig. 5(c) presents MATLAB/SIMULINK Design of IEEE 39-bus power system. All data of this power system can be found in (Khodabakhshian *et al.* 2013). Furthermore, a Doubly Fed Induction Generator (DFIG) based wind turbine has provided the required power of bus no. 16. DFIG is the most predominant topology for wind turbines that has provided the required power of global and local power systems factor (Shehata *et al.* 2015). DFIG has been generally constructed by wound rotor asynchronous machine and partial-scale back-to-back converter that makes it more operational in wide range of wind speeds (Abdelmalek *et al.* 2016).

4.5 Interconnected multi area power systems considering attendance of FOPID–SSSC

Alleviating the Area Control Error (ACE) in all areas of the interconnected multi area system is recognized as the most important issue related to load frequency control. Both the frequency and tie-line power deviations are two prominent criteria of ACE that can be expressed as follows (Divya *et al.* 2005, Goshal 2004):

$$ACE_i = \sum_j \Delta P_{tie,\,i,j} + B_i\Delta f_i \quad (53)$$

Where, B_i indicates the bias factor of system frequency from *ith* area, Δf_i indicates the error of system frequency from *ith* area, and also $\Delta P_{tie,i,j}$ indicates the tie-line power deviations between the *ith* and *jth* areas.

Form the Laplace domain viewpoint, output signal of AGC can be figured out
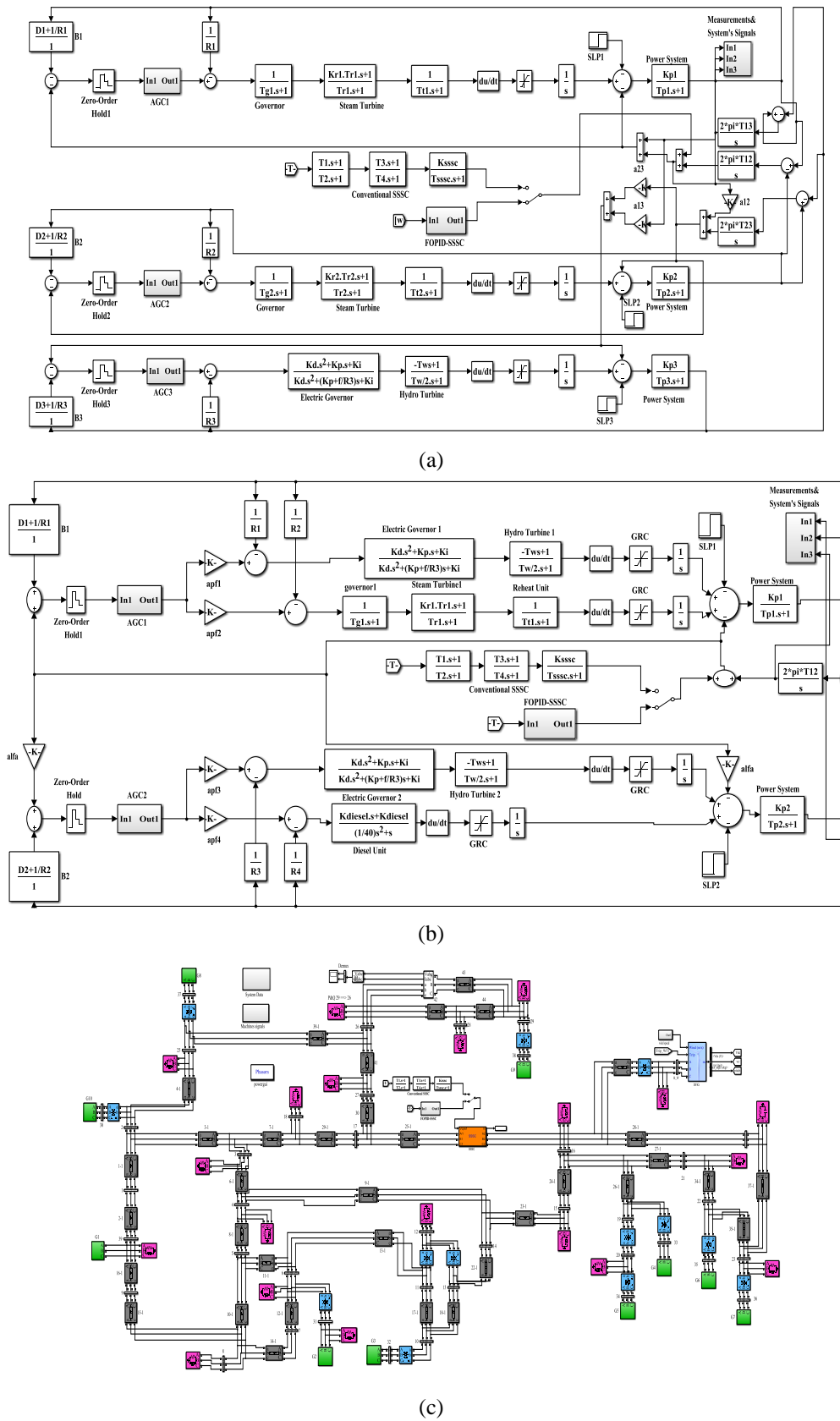
(a)

(b)

(c)

Fig. 5(a) Transfer function of three area hydro-thermal system, (b) Transfer function of two area hydro-thermal-diesel system and (c) IEEE 39-bus ten-machine New-England power system

$$-G_{AGC,i}(s).ACE_i(s) \tag{54}$$

To more verify and validate the dynamic performance of FOPID–SSSC, a conventional controller based SSSC has been thoroughly appraised along with it.

The parameters of these controllers that are determined to be optimized by MOBA are:

– FOPID–SSSC: $K_{P,SSSC}$, $K_{I,SSSC}$, $K_{D,SSSC}$, λ, μ
– Conventional controller based SSSC: K_{SSSC}, T_{SSSC}, T_1 and T_3

While, $T_2=T_4=0.1$.

4.6 Objective functions

Heretofore, many different criterions such as ITAE, IAE, ISE, and ITSE have been widely applied in order to appraise the control performance.

For all that, an effectual criterion is here introduced to perform the simultaneous optimization scheme i.e., *F* in order to scrutinize the controllers' performance. This criterion for the frequency and tie-line power deviations can be presented as follows (Falehi *et al.* 2011, Falehi 2013)

$$J_f = \int_{t=0}^{t=t_{sim}} \left(\sum |\Delta f_i| \right) t.dt \tag{55}$$

$$J_P = \int_{t=0}^{t=t_{sim}} \left(\sum |\Delta p_{tie,i,j}| \right) t.dt \tag{56}$$

$$F_f = \sum_{i=1}^{N_p} J_{f,i} \tag{57}$$

$$F_P = \sum_{i=1}^{N_p} J_{P,i} \tag{58}$$

Where, N_P and t_{sim} are respectively SLP number and time period of simulation. J_f and J_P indicate two important criteria related to controlling the dynamic stability. F_f and F_P also indicate the held forth objective functions scheduled for simultaneous optimization in order to suppress both the dynamic oscillations of frequency and tie-line power deviation. Further to that, the optimization problem can be presented by

$$Minimize \; F_f \; \& \; F_P \tag{59}$$

Subject to

$$K_{SSSC}^{min} \leq K_{SSSC} \leq K_{SSSC}^{max}, \; T_{SSSC}^{min} \leq T_{SSSC} \leq T_{SSSC}^{max},$$

$$T_1^{min} \leq T_1 \leq T_1^{max}, T_3^{min} \leq T_3 \leq T_3^{max}$$

$$K_P^{min} \leq K_P \leq K_P^{max}, \; K_I^{min} \leq K_I \leq K_I^{max}, \tag{60}$$

$$K_D^{min} \leq K_D \leq K_D^{max}, \lambda^{min} \leq \lambda \leq \lambda^{max}, \mu^{min} \leq \mu \leq \mu^{max}$$
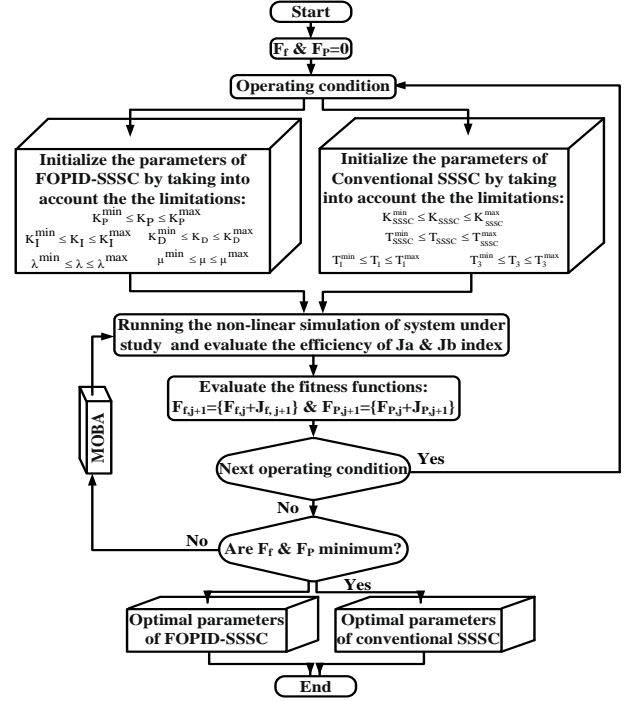

Fig. 6 MOBA based simultaneous optimization scheme

Likewise, Fig. 6 presents the simultaneous optimization flowchart with occurrence of 1% SLP in each area of the interconnected multi-area power systems.

5. Results and discussions

5.1 Interconnected two-area hydro-thermal-diesel system

To provide appropriate bed in order to deal with the dynamic performance of FOPID–SSSC, this power system is affected by 1% SLP in both areas. The simultaneous optimization strategy is carried out for FOPID–SSSC as well as the conventional controller based SSSC considering the held forth objective function with respect to two SLP. Optimum parameters of these controllers resulted from the optimization scheme are given in Tables 1 and 2. Also, Fig. 7(a) portrays the Pareto front resulted from MOBA.

Table 1 FOPID–SSSC's optimum parameters related to the interconnected two-area hydro-thermal-diesel system

$K_{P,SSSC}$	$K_{I,SSSC}$	$K_{D,SSSC}$	λ	μ
0.10951	0.02335	0.17953	0.84183	1.15829

Table 2 Conventional controller based SSSC's optimum parameters related to the interconnected two-area hydro-thermal-diesel system

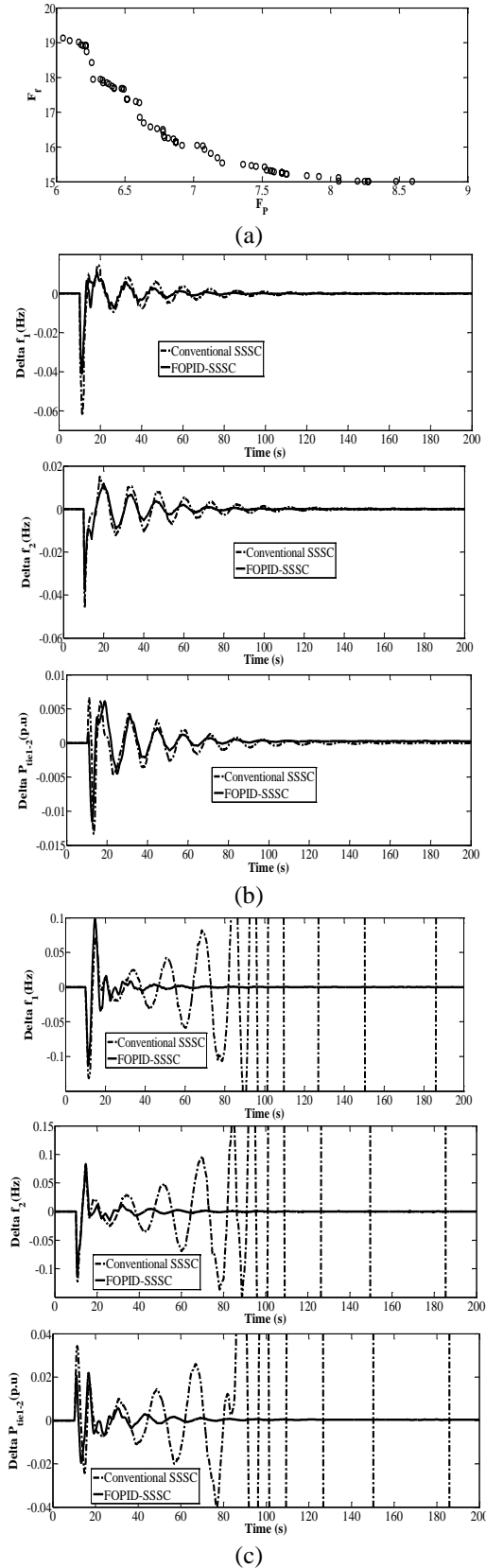| K_{SSSC}	T_{SSSC}	T_1	T_3
0.14784	0.46062	0.03677	0.063015

(a)

(b)

(c)

Fig. 7 (a). Pareto optimization front resulted from MOBA and (b) Response of affected interconnected two-area hydro-thermal-diesel system under 1% SLP in area1 and (c) Response of affected interconnected two-area hydro-thermal-diesel under 3% SLP in area 2

Finishing the optimization process, high compensation capability of FOPID–SSSC in order to control the power flow of tie-line power is well corroborated, whereby, the dynamic stability of interconnected two-area hydro-thermal-diesel system is appropriately attained, that hereunder parts point to this result.

5.1.1 Affected power system caused by SLP in area 1

1% SLP occurs in area 1 at t=10s to appraise the effectiveness of controllers, and then, MOBA is here responsible for the simultaneous optimum tune of the controllers' parameters. Fig. 7(b) demonstrates the system simulation response. What is certain is that the aforementioned expectation is well proofed. As can be seen, all the stability benchmarks i.e., settling-time, overshoot, undershoot and steady-state error of tie-line power and frequency are considerably reduced when FOPID–SSSC is indwelled in the system. Thus, FOPID–SSSC can significantly improve the dynamic stability of the interconnected two-area hydro-thermal-diesel system as compared to the conventional controller based SSSC.

5.1.2 Affected power system caused by SLP occurrence in area 2

In this section, 3% SLP in area 2 impacts this system at t=10s. Since this perturbation has highly affected the power system and caused the system gone into the instable status, it provides an appropriate bed to scrutinize and figure out the compensation capability of FOPID–SSSC in order to bring back this system into the stable condition. Fig. 7(c) shows that the conventional controller based SSSC cannot bring back the disturbed interconnected two-area hydro-thermal-diesel system resulted from this great perturbation into the stable condition, whereas FOPID–SSSC can vanquish the problem, and then, bring back this system in to the stable state.

5.2 Interconnected three-area hydro-thermal system

Similar to the previous section, FOPID–SSSC is thoroughly appraised in interconnected three-area hydro-thermal system with consideration of perturbation in all areas. Following solution of the simultaneous optimization scheme, FOPID–SSSC's optimum parameters as well as conventional controller based SSSC's optimum parameters are figured out that are respectively brought in Table 3 and Table 4. Meantime, Fig. 8(a) portrays Pareto front resulted from MOBA.

Anyhow, the results of following sections have clearly demonstrated and corroborated the compensation performance of FOPID–SSSC in order to stabilize the interconnected three-area hydro-thermal system.

Table 3 FOPID–SSSC's optimum parameters related to interconnected three-area hydro–thermal system

$K_{P,SSSC}$	$K_{I,SSSC}$	$K_{D,SSSC}$	λ	μ
0.1258	0.091738	0.19912	0.86292	1.29735

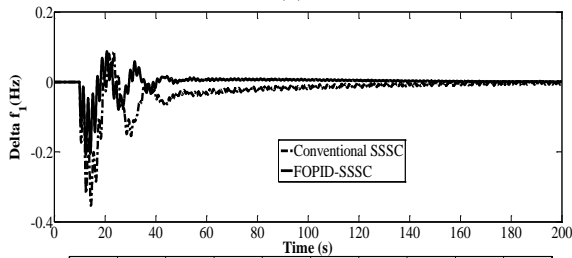Table 4 Conventional controller based SSSC's optimum parameters related to interconnected three-area hydro–thermal system

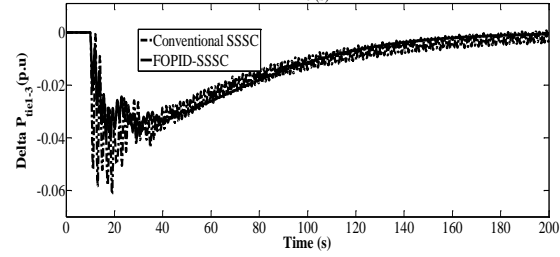| K_{SSSC}	T_{SSSC}	T_1	T_3
0.19948	0.5769	0.18610	0.11206

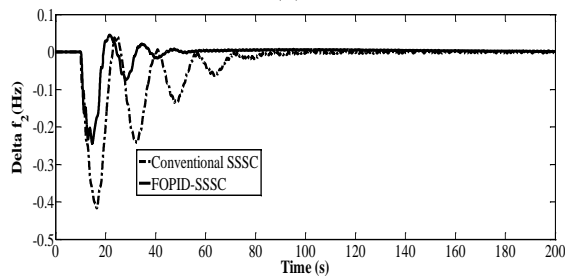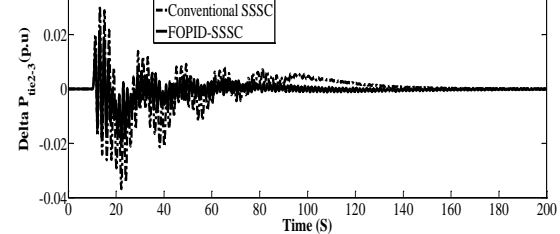### 5.2.1 Affected power system caused by SLP occurrence in area 1
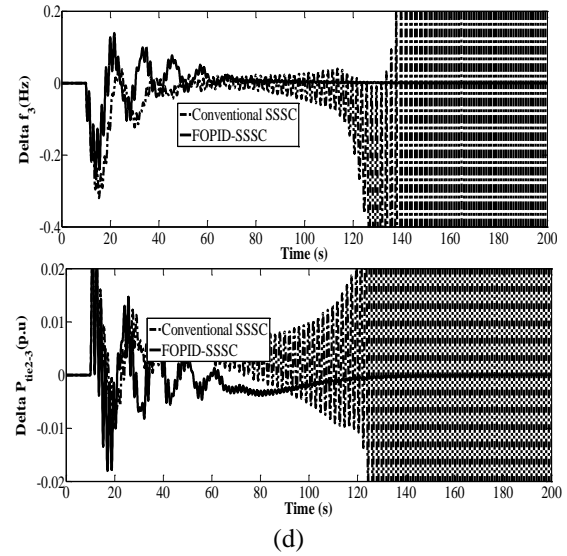
(a)

(b)

(c)

Continued-

(d)
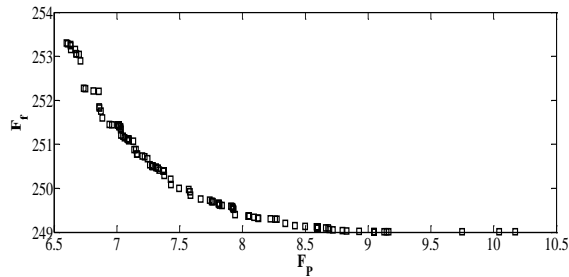
Fig. 8 (a) Pareto optimization front resulted from MOBA, (b) Response of affected interconnected three-area hydro-thermal system caused by 3% SLP in area 1, (c) Response of affected interconnected three-area hydro-thermal system caused by 3% SLP in area 2 and (d) Response of affected interconnected three-area hydro-thermal system caused by 4% SLP in area 3

5.2.2 Affected power system caused by SLP occurrence in area 2

5.2.3 Affected power system caused by SLP occurrence in Area 3

5.3 IEEE 39-bus 10-machine New England Power System

This large-scale power system is here taken into account to more verify and validate the compensation capability of FOPID–SSSC to suppress the dynamic oscillations of frequency and tie-line power deviations. It is also considered that DFIG to be located in bus no. 16, while, the power system is faced fault occurrence in bus no.14 at t=1s. This fault is cleared after 8 cycles. When the MOBA based optimization problem is solved, FOPID–SSSC's optimum parameters as well as conventional controller based SSSC's optimum parameters are figured out and respectively given in Tables 5 and 6. Meantime, Fig. 9(a) portrays the Pareto front resulted from MOBA.

Table 5 FOPID–SSSC's optimum parameters related to IEEE 39-bus 10-machine New-England power system

$K_{P,SSSC}$	$K_{I,SSSC}$	$K_{D,SSSC}$	λ	μ
20.6821	0.4588	0.2944	0.9065	1.3142

Table 6 Conventional controller based SSSC's optimum parameters related to IEEE 39-bus 10-machine New-England power system

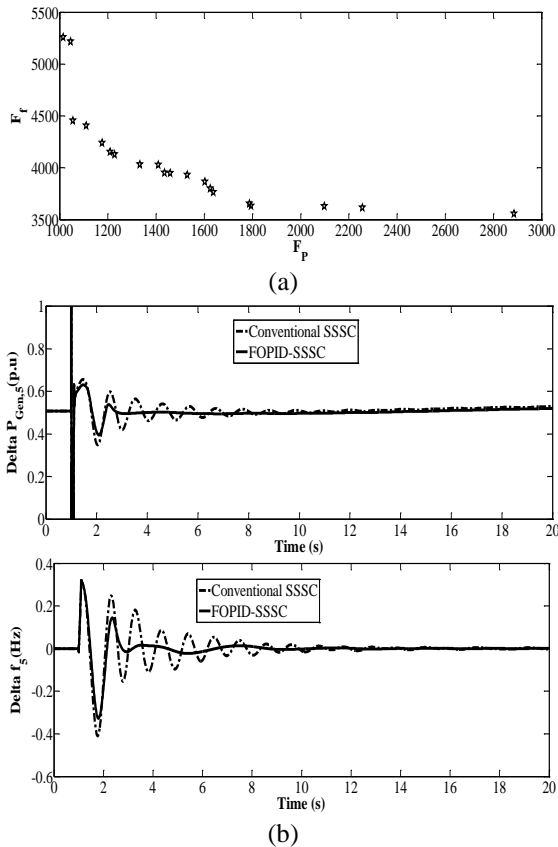| K_{SSSC}	T_{SSSC}	T_1	T_3
0.8072	0.9379	0.3157	0.5963

Fig. 9 (a) Pareto optimization front resulted from MOBA and (b) Response of affected IEEE 39-bus 10-machine New-England power system caused by fault occurrence in bus no.14

6. Conclusions

This paper presents a high dynamic performance FOPID–SSSC aimed to quickly stabilize the affected interconnected multi-area multi-source system. Both the critical issues in this regard i.e., the frequency and the tie-line power deviations are formularized in the form of a multi-object problem, and accordingly their dynamic oscillations have been suppressed. Meanwhile, MOBA based simultaneous optimization scheme has been scheduled with respect to the perturbation occurrence in all areas of the interconnected multi-area power systems. Three different interconnected multi-area power systems, that is to say: two-area hydro-thermal-diesel, three-area hydro-thermal and IEEE 39-bus 10-machine new-England power system are applied to provide an appropriate bed to evaluate the compensation capability of FOPID–SSSC aimed at sustaining the power system stability. Ultimately, the simulation results of all three interconnected multi-area power systems have clearly demonstrated the composition capability of FOPID–SSSC as compared to the conventional controller based SSSC in order to enhance the power system dynamic stability.

References

Abdelmalek, S., Barazane, L. and Larabi, A. (2016), "A novel scheme for current sensor faults diagnosis in the stator of a DFIG described by a T-S fuzzy model", *Measurement*, **91**(9), 680-691.

Alomoush, M.I. (2010), "Load frequency control and automatic generation control using fractional-order controllers", *Electrical Engineering*, **91** (7), 357-368.

Balarko, C., Bikash, C., Aygyrios, C., Zolotas, Jaimoukha, M. and Green, C. (2003), "Mixed-sensitivity approach to H∞ control of power system oscillations employing multiple FACTS devices", *IEEE T. Power Syst.*, **18**(3), 1149-1156.

Bevarani, H., Hiyama, T. and Mitani. Y. (2008), "Power system dynamic stability and voltage regulation enhancement using an optimal gain vector", *Control Eng. Pract.*, **16**(9), 1109-1119.

Bhatt, P., Roy, R. and Ghoshal, S.P. (2011), "Comparative performance evaluation of SMES–SMES, TCPS–SMES and SSSC–SMES controllers in automatic generation control for a two–area hydro–hydro system", *Elec. Power Energ. Syst.*, **33** (6), 1585-1597.

Cai, L. and Erlich, I. (2005), "Simultaneous coordinated tuning of PSS and FACTS damping controllers in large power systems", *IEEE T. Power Syst.*, **20**(1), 294-300.

Chakraborty, J., Konar, A., Nagar, A. and Das, S. (2009), "Rotation and translation selective Pareto optimal solution to the box-pushing problem by the mobile robots using NSGA-II", *IEEE Congress In: Evolutionary Computation.*

Chaudhuri, B. and Pal, B. (2004), "Robust damping of multiple swings modes employing global stabilizing signals with TCSC", *IEEE T. Power Syst.*, **19**(1), 499-506.

Chaudhuri, B., Pal. B., Zolotas, AC., Jaimoukha, I.M. and Geen, TC. (2003), "Mixed-sensitivity approach to H control of power systems oscillations employing multiple FACTS devices", *IEEE T. Power Syst.*, **18**(3), 1149-1156.

Debbarma, S., Saikia, L.C. and Sinha, N. (2014), "Automatic generation control using two degree of freedom fractional order PID controller", *Elec. Power Energ. Syst.*, **58**(1), 120–129.

Divya, K.C. and Nagendra Rao. P.S. (2005), "A simulation model for AGC studies of hydro–hydro systems", *Elec. Power Energy Systems*, **27** (2), 335–342.

Falehi, A.D. (2012), "Simultaneous coordinated design of TCSC-based damping controller and AVR based on PSO technique", *PRZEGLĄD ELEKTROTECHNICZNY (Electrical Review)*, **88** (5), 0033-2097.

Falehi, A.D. and Rostami, M. (2011), "Design and analysis of a novel dual-input PSS for damping of power system oscillations Employing RCGA-Optimization Technique", *Int. Rev. Elec. Eng.*, **6**(2), 938-945.

Falehi, A.D., Dankoob, A., Amirkhan, S. and Mehrjardi, H. (2011), "Coordinated design of STATCOM-based damping controller and dual-input PSS to improve transient stability of power system", *Int. Rev. Elec. Eng.*, **6**(3), 1308-1318.

Falehi, A.D., Rostami, M. and Doroudi, A. (2011), "'Coordinated design of PSSs and SSSC-based damping controller based on GA optimization technique for damping of power system multi-mode oscillations", *IEEE PEDSTC Conference*, 199-204.

Falehi, A.D., Rostami, M., Doroudi, A. and Ashrafian, A. (2012), "Optimization and coordination of SVC-based supplementary controllers and PSSs to improve the power system stability using genetic algorithm", *Turk J Elec Eng. Comp. Sci.*, **20**(5), 639-654.

Falehi, A.D> (2013), "Design and scrutiny of maiden PSS for alleviation of power system oscillations using RCGA and PSO techniques", *J. Elec. Eng. Technol.*, **8**(3), 402-410.

Goshal, S.P. (2004), "Optimization of PID gains by particle swarm optimization in fuzzy based automatic generation control", *Elec. Power Syst. Res.*, **72**(1), 203-212.

Gyugyi, L. (1992), "Unified power-flow control concept for flexible AC transmission systems", *IEE Proc. Gener. Transm. Distrib.*, **139** (4), 323–331.

Gyugyi, L., Schauder, C.D. and Sen, K.K. (1997), "Static synchronous series compensator: a solid-state approach to the series compensation of transmission lines", *IEEE T. Power Deliver*, **12**(1), 406-417.

Iracleus, D.P. and Alexandridis. A.T. (2005), "A multi-task automatic generation control for power regulation", *Elec. Power Syst. Res.*, **73**(1), 275-285.

Kazemi, M.R., Motlagh, J. and Naghshbandi. A.H. (2007), "Application of a new multi-variable feedback linearization method for improvement of power systems transient stability", *Elec. Power Energ. Syst.*, **29**(3), 322-328.

Khodabakhshian, A. and Hemmati, R. (2013), "Multi-machine power system stabilizer design by using cultural algorithms", *Elec. Power Energ. Syst*, **44**(1), 571-580.

Khuntia, S.R. and Panda, S. (2013), "ANFIS approach for SSSC controller design for the improvement of transient stability performance", *Math. Comput. Model.*, **57**(2), 289-300.

Kundur, P., Klein, M., Rogers, G.J. and Zywno, M.S. (1989), "Application of power system stabilizers for enhancement of overall system stability", *IEEE T. Power Syst.*, **4**(2), 614-626.

Lu, B. (2012), "The first integral method for some time fractional differential equations", *J. Math. Anal. Appl.*, **395**(2), 684-693.

Moradi, A. Shirazi, K.H., Keshavarz, M., Falehi, A.D. and Moradi, M. (2014), "Smart piezoelectric patch in nonlinear beam: design, vibration control and optimal location", *T. Inst. Msurement Control*, **36**(1), 131-144.

Panda, S. (2011), "Differential evolution algorithm for SSSC-based damping controller design considering time delay", *J. Franklin Inst.*, **348**(3), 1903-1926.

Panda, S., Swain, S.C., Rautray, P.K., Malik, R.K. and Panda, G. (2010), "Design and analysis of SSSC-based supplementary damping controller", *Simul. Model. Pract. Th.*, **18**(9), 1199-1213.

Pham, D.T. and Castellani, M. (2009), "The bees algorithm: Modelling foraging behaviour to solve continuous optimization problems", *Sage J.* **223**(12), 2919-2938.

Pham, D.T., Ghanbarzadeh, A., Koc, E., Otri, S., Rahim, S. and Zaidi, M. (2006), "The bees algorithm, a novel tool for complex optimisation problems", *Proceedings of the 2nd Int Virtual Conf on Intelligent Production Machines and Systems.*

Pham, D.T., Koc, E., Ghanbarzadeh, A. and Otri, S. (2006), "Optimisation of the Weights of Multi-Layered Perceptions Using the Bees Algorithm", *Proceedings of 5th International Symposium on Intelligent Manufacturing Systems, Sakarya, Turkey*, 38–46.

Pham, D.T., Otri, S., Ghanbarzadeh, A. and Kog, E. (2006), "Application of the bees algorithm to the training of learning vector quantisation networks for control chart pattern recognition", *ICTTA'06 Information and Communication Technologies*, 1624-1629.

Sabatier, J., Lanusse, P., Melchior, P. and Oustaloup, A. (2015), "Fractional order differentiation and robust control design", *Intelligent Systems, Control and Automation: Science and Engineering*, **77**.

Shehata, E.G. (2015), "Sliding mode direct power control of RSC for DFIGs driven by variable speed wind turbines", *Alexandria Eng. J.*, **54**(4), 1067-1075.

Swain, S.C., Panda, S. and Mahapatra, S. (2015), "A multi-criteria optimization technique for SSSC based power oscillation damping controller design", *Ain Shams Eng. J.*, **6**(1), 1-13.

Taibin, C., Rui, H. and Bifu, Q. (2011), "The design of nonlinear control strategy for SSSC based on constant voltage control", *International IEEE Conference on Control and Industrial Engineering* (CCIE), 30-32.

Tan, W. and Xu, Z. (2009), "Robust analysis and design of load frequency controller for power systems", *Elec. Power Syst. Res.*,**79**(3), 846-853.

Tereshko, V. and Loengarov, A. (2005), "Collective decision making in honey bee foraging dynamics", *Comput. Inform. Syst.*, **9**(3), 1-7.

Truong, D.N. and Ngo, V.T. (2015), "Designed damping controller for SSSC to improve stability of a hybrid offshore wind farms considering time delay", *Elec. Power Energ. Syst.*, **65**(4), 425-431.

Truong, D.N. and Ngo, V.T. (2015), "Designed damping controller for SSSC to improve stability of a hybrid offshore wind farms considering time delay", *Elec. Power Energ. Syst.*, **65**(2), 425-431.

Xue, D. and Chen, YQ. (2002), "A comparative introduction of four fractional order controllers", *Proceedings of the 4th World Congress on Intelligent Control and Automation*, 3228-3235.

Zamani, M., Ghartemani, MK., Sadati, N. and Parniani, M. (2009), "Design of a fractional order PID controller for an AVR using particle swarm optimization", *Control Eng. Pract.*, **17**(12), 1380-1387.

HJ

Appendix

A. Interconnected Three-Area Hydro-Thermal Systems

f = 60Hz; T_{gi} = 0.08s; T_{ri} = 10s; H_i = 5s; T_{ti} = 0.3s; K_r = 0.5; P_{ri} = 2000MW; T_{pi} = 20s; K_d = 4.0, K_p = 1.0, K_i = 5.0; D_i = 0.1283 p.u.MW/Hz; K_{pi} = 120 Hz/p.u MW, T_w=1s, a_{12} = a_{13} = a_{23} =-1.

B. Interconnected Two-Area Hydro-Thermal-Diesel System

K_{P1}= K_{p2}=120 Hz/p.u MW, R_1=R_2= R_3=R_4=2.4 Hz/ p.u MW, T_g=0.08 s, T_T=0.3 s, T_R=5s, T_W=1s, K_P=1.0, K_i=5.0, K_d=4.0, D_i = 0.00833 p.u.MW/Hz, T_w=1.0 s, P_{R1}=1800 MW, P_{R2}=1200 MW, $G_D = \dfrac{16.5s + 16.5}{(1/40)s^2 + s}$